GHENT UNIVERSITY

FACULTY OF ENGINEERING AND ARCHITECTURE

E044821A - FEM and Constitutive Material Laws in Structural Engineering

---

Project: Concrete Deep Beam

Group 2:

Eva De Jaeger
Rian Denys
Karlijn Geys
Thomas Meyers

December 2nd 2020

Prof. Dr. Ir. Diego Allaix
Dr. Ir. Wouter Botte

Contents

1 Introduction **2**
- 1.1 Structure . . . 2
- 1.2 Experimental test . . . 2
- 1.3 Objective of the analysis . . . 2

2 Finite Element model **3**
- 2.1 Boundary conditions and loading . . . 3
- 2.2 Material models and parameters . . . 4
  - 2.2.1 Concrete . . . 4
  - 2.2.2 Reinforcement steel . . . 4
  - 2.2.3 Steel plates . . . 5
- 2.3 Loading scheme and schedule . . . 5
- 2.4 Type and number of finite elements . . . 6

3 Linear elastic analysis and strut and tie model **6**
- 3.1 Linear analysis . . . 6
  - 3.1.1 Reaction force . . . 6
  - 3.1.2 Displacement . . . 7
  - 3.1.3 Stress field S_{xx}, S_{yy} and S_{xy} . . . 7
  - 3.1.4 Conclusion . . . 7
- 3.2 Strut and tie model . . . 8
  - 3.2.1 Type of model . . . 8
- 3.3 Load bearing capacity . . . 10
- 3.4 Comparison and conclusion . . . 13

4 Non-linear analysis **13**
- 4.1 Results of a non-linear analysis until failure . . . 13
  - 4.1.1 Load-deflection curve . . . 14
  - 4.1.2 Reinforcement stresses/crack widths . . . 15
- 4.2 Influence of mesh size and type of element . . . 18
  - 4.2.1 Mesh sizes . . . 18
  - 4.2.2 Comparison between sizes/shapes . . . 19
  - 4.2.3 Number of elements per mesh shape . . . 20
  - 4.2.4 Conclusion of the non-linear analysis . . . 21

5 Conclusion and summary **21**

6 References **22**

1 Introduction

1.1 Structure

The investigated beam is *B3.0A-4*. This beam, as well as the relevant information about the geometrical properties of the structure, material properties, load arrangement and test layout, is described in the paper *"Experimental Studies on High-Strength Concrete Deep Beams"*. The geometry and dimensions of the structure and the location and dimensions of the reinforcements in the beam are illustrated in Figure 1.

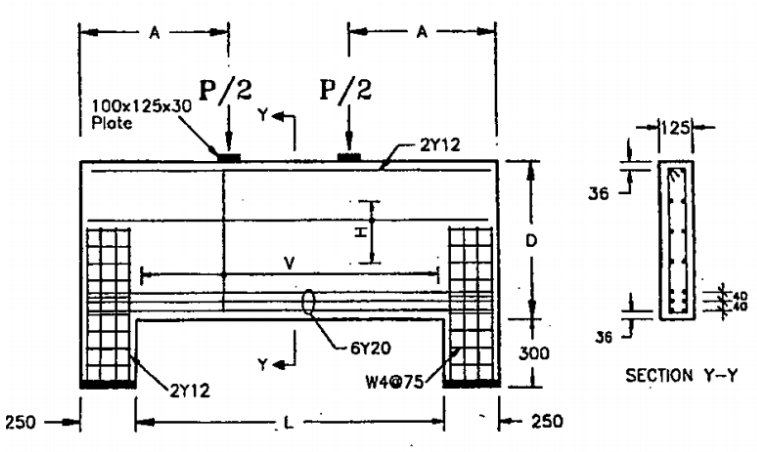

Figure 1: Dimension for Beam *B3.0A-4*

The parameters for the investigated beam *B3.0A-4* can be found in Table 1. The dimensions that were not given in the paper are assumed and based on the other dimensions that are given.

Table 1: Dimensions and details of beam

Beam	**L [mm]**	**A [mm]**	**D [mm]**	**Web Reinforcement**	
B3.0A	2100	925	700	V: 29x2W6	H: 3x2W6

1.2 Experimental test

The described beam is supported on two steel plates at the end of the beam. Two loads are placed on a distance $A = 925\,mm$ from each side. The load is applied vertically via a spherical seat, using a 3000 kN capacity hydraulic jack. Strains are measured along the main tension reinforcement and along three stirrups using strain gauges. The beam is loaded with increments of 100 kN until failure occurs, with the measured displacements and strains measured and cracks marked.

1.3 Objective of the analysis

The goal of this assignment is to develop a 2D plane stress model of a concrete deep beam and to perform a FE analysis, first using a linear elastic analysis and secondly taking into account the non-linear material behaviour.

The obtained, theoretical results can be compared to the experimental results regarding the load-deflection curves, the crack patterns and the reinforcement stresses. Also the difference in using different mesh sizes or different shapes of the mesh elements (triangular vs quadrilateral) will be looked at. The optimal combination can then be chosen based on the best approximation of the theoretical situation to the experimental one.

2 Finite Element model

2.1 Boundary conditions and loading

The program used in this assignment is DIANA. DIANA stands for "DIsplacement ANAlyser" and is a Finite Element Analysis (FEA) solver that does basic and advanced analysis of various structures.

To avoid high stress concentrations at the locations of the loads and supports, two steel plates are added. The model is loaded with a basic force of -1 kN (which will be multiplied with a loading factor in the load steps). During the analysis, the self weight is neglected because it will not have any significant influence on the results.

The structure is symmetrical, so it is decided to model only half of the structure by applying symmetric boundary conditions. The beam is supported at the symmetry axis by a line support, restricting the movement in the x-direction and on the other side by a simple support, restricting the movement in the y-direction. This gives the advantage of faster execution of the calculations, but assumes the failure mode is symmetric. The model of the structure in DIANA is displayed in Figure 2.

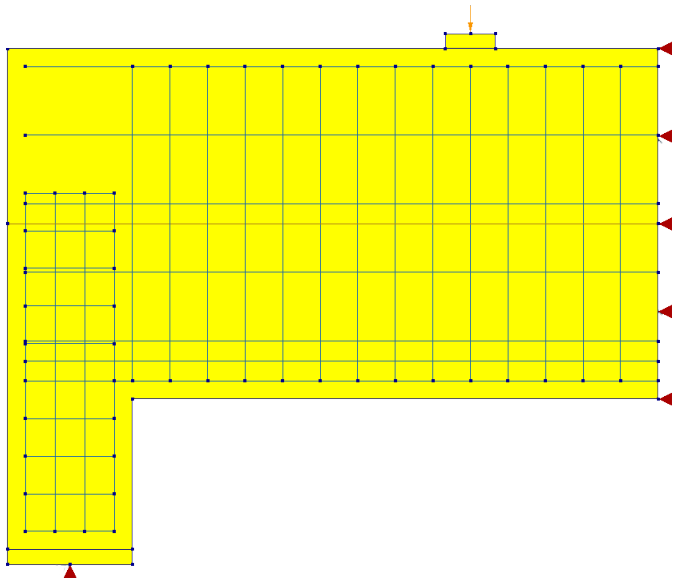

Figure 2: Model with boundary conditions and applied load

The use of a model with half the structure is substantiated by Figure 3a. The entire model is hinged on the left. On the right, roller bearings are defined. Although Figure 3b reflects reality better, the difference between the two is negligible. Therefore, further calculations are made with half the model in order to minimise calculation times.

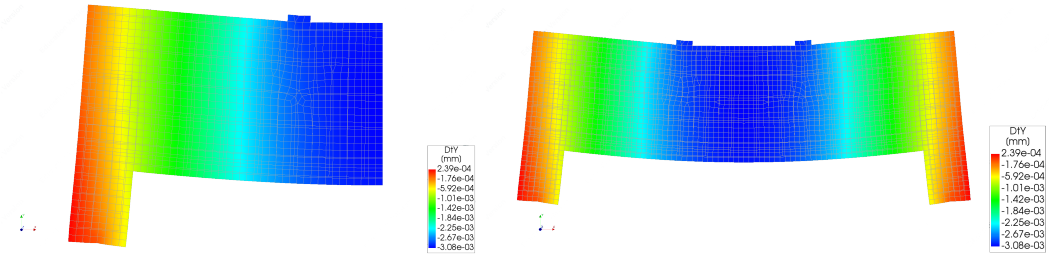

(a) Half the structure (b) Entire structure

Figure 3: Model: Vertical displacements

2.2 Material models and parameters

2.2.1 Concrete

The material properties of the concrete used to construct the beam are given in Table 2. The parameters are determined based upon a concrete cylinder (300 mm high by 150 mm diameter). The samples are poured together with the beam and tested 75 days later at the time of the experiment.

Table 2: Properties of concrete

	Symbol	**Value**	**Unit**
Linear material properties			
Young's modulus	E	50700	N/mm^2
Poisson ratio	ν	0.3	[-]
Mass density	ρ	2520	kg/m^3
Total strain-based crack model			
Crack orientation		rotating	
Tensile behaviour			
Tensile curve		Hordijk	
Tensile strength	f_{ct}	6.59	N/mm^2
Mode-I tensile fracture energy	G_F	$= 73 \cdot f_{cm}^{0.18} = 0.163$	N/mm
Crack bandwidth specification		Rots	
Poisson's ratio reduction model		No reduction	
Compressive behaviour			
Compressive curve		Thorenfeldt	
Compressive strength	f_{cm}	88	N/mm^2
Lower bound reduction curve		0.6	[-]
Reduction model due to lateral cracking		Vecchio and Collins 1993	
Stress confinement model		No increase	

2.2.2 Reinforcement steel

The main steel reinforcement consists of nominal 400 MPa deformed Y-bars. The web reinforcement and column ties are fabricated from hard drawn wire having a nominal yield strength of 450 MPa and are denoted as W-bars.

Table 3: Model parameters of reinforcement steel

	Symbol	**Value**	**Unit**
Linear material properties			
Young's modulus	E	193000	N/mm^2
Von Mises plasticity			
Plastic hardening		No hardening	

Table 4: Reinforcement steel properties

Bar	**d** $[mm]$	**A** $[mm^2]$	$2 \cdot A\ [mm^2]$	$\sigma_y\ [N/mm^2]$	$E_0\ [kN/mm^2]$
W4	4.09	13.14	26.28	580	215
W6	6.3	31.17	62.35	590	193
Y12	11.2	98.52	197.04	440	195
Y20	20	314.16	628.32	440	201

2.2.3 Steel plates

The supports and load plates are modelled as steel plates.

Table 5: Model parameters of steel plates

	Symbol	**Value**	**Unit**
Young's modulus	E	210000	N/mm^2
Poisson ratio	ν	0.3	[-]
Mass density	ρ	7850	kg/m^3

The plates are connected with a 2D line interface. The characteristics are determined using the general guidelines for [8].

Table 6: Model parameters of interface

	Symbol	**Equation**	**Value**	**Unit**
Normal stiffness modulus	K_n	$100 \cdot \frac{E_{concrete}}{l_{element}}$	190000	N/mm^2
Shear stiffness modulus	K_t	$\frac{K_n}{10}$	19000	N/mm^2

The parameter $l_{element}$ is the characteristic length of an element. The initial value of the mesh element size is considered.

2.3 Loading scheme and schedule

The load scheme is determined as follows: the load increment that leads to the first crack is 210 kN, so it is decided that a load step of half of this value, rounded 100 kN, is taken. This means that first a step of 100 kN is used and then steps of 50 kN.

The first load scheme is thus 100.000 50.000(15). This gives a P_u of 1100 kN. Then, it is refined to 100.000 50.000(8) 5.000(2) 1.000(10), which gives a more accurate P_u of 1026 kN.

Table 7: Model parameters of loads

Load steps	
Step sizes	100 50(15) *initially*
Arc length control	OFF
Equilibrium iteration	
Method	Newton-Rhapson
Type	Regular
First tangent	Tangential
Convergence norm	Energy
Energy settings	
Convergence tolerance	0.005
Abort criterion	10000
Termination at non-convergence	Continue
Solution method	
Method	Parallel Direct Sparse

The convergence norm is set on 'Continue'. This is only allowed if the non-converged steps are followed by converged steps, which is indeed the case.

2.4 Type and number of finite elements

The mesh of the linear and first non-linear analysis has an element size of 30 *mm*. This is the value of the smallest dimension of the beam which is the height of the load plate. The mesh type is hexa-quad, which means the shape of the elements is quadrilateral. The Technical Document of the *Rijkswaterstaat* [4] specifies minimum and maximum values of the element size. A more detailed analysis of the mesh is conducted in Section 4.2.

3 Linear elastic analysis and strut and tie model

In this section a linear analysis of the structure is performed. Based on the results of the analysis, a strut-and-tie model is defined.

3.1 Linear analysis

In this linear analysis the reaction force, the total displacement and the stress field are examined. Several plots are made to check whether the model in DIANA behaves as expected.

3.1.1 Reaction force

To validate the results of the model, a check of the reaction force is done. When applying a load, it is expected that the reaction forces are divided equally between the two supports and are therefore equal to *P/2*. Since the load has only a vertical component, a check of the reaction forces is done along the Y-axis. When looking to Figure 4, one can say that this statement is indeed valid.

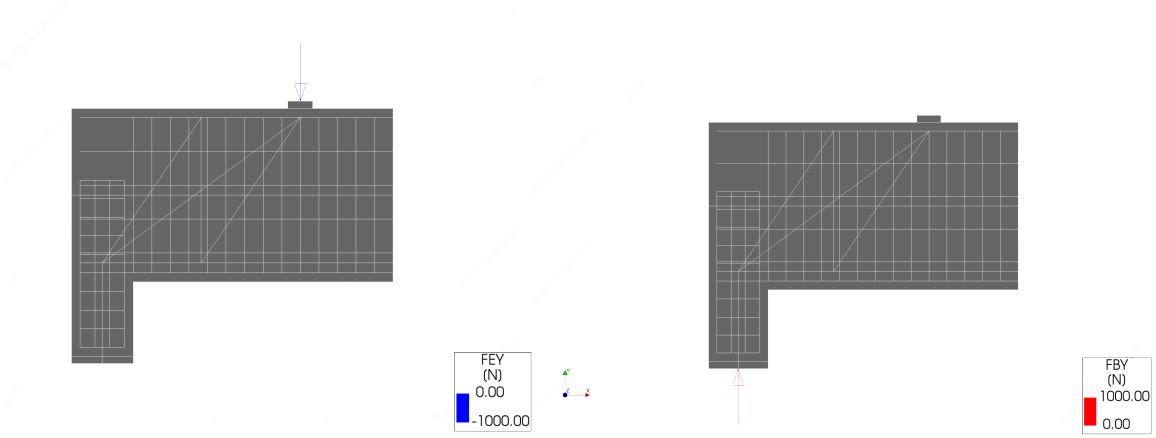

(a) Load on model (b) Reaction on model

Figure 4: Reaction force due to a force P of 2 kN

3.1.2 Displacement

On Figure 5, a contour plot of the displacements in the vertical displacement is shown. The largest vertical displacements are, as expected, in the middle of the span. The left part rises a little bit when the force is added.

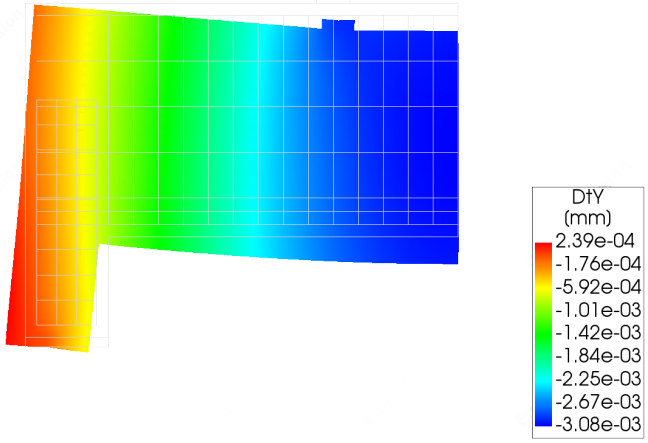

Figure 5: Displacement DTy due to a force P of 2 kN

3.1.3 Stress field S_{xx}, S_{yy} and S_{xy}

Different stress fields are plotted on Figure 6. Figure 6a shows the stresses in the x direction. The tensile stresses at the bottom of the beam are clearly visible and at the upper part of the beam, compression stresses are present. Figure 6b shows the stresses in the y-direction. Under the load plate and above the support, compression stresses are visible. This plot shows the importance of the steel plates to avoid locally high concentrated stresses.

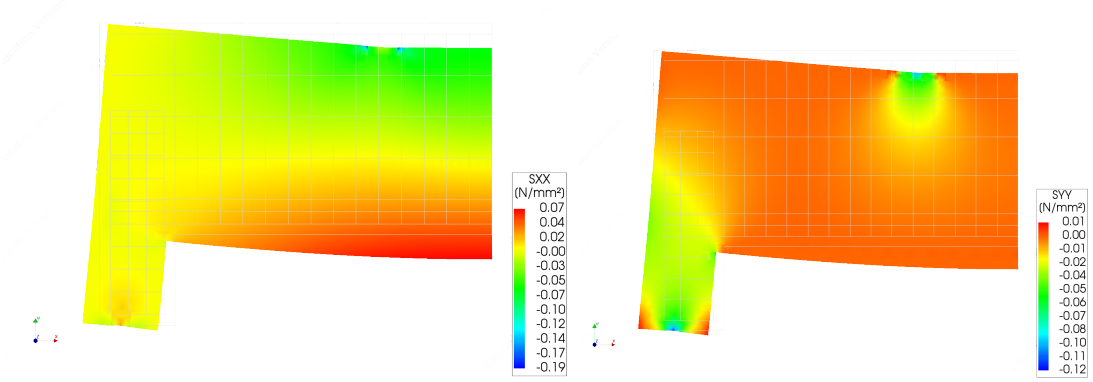

(a) S_{xx} (b) S_{yy}

Figure 6: Stress fields due to a load P of 2 kN

3.1.4 Conclusion

After this process is done, it can be concluded that the structure behaves as expected. This is important for the following sections.

3.2 Strut and tie model

3.2.1 Type of model

The force transfer in concrete beams is schematized with the help of struts and ties. This strut-and-tie-model is determined from the elastic stress distribution in the considered beam. Looking at the stress trajectories, a simple reinforcement arrangement can be made. The plot in Figure 7 shows the trajectories in the beam, subjected to a force of 700 *kN*.

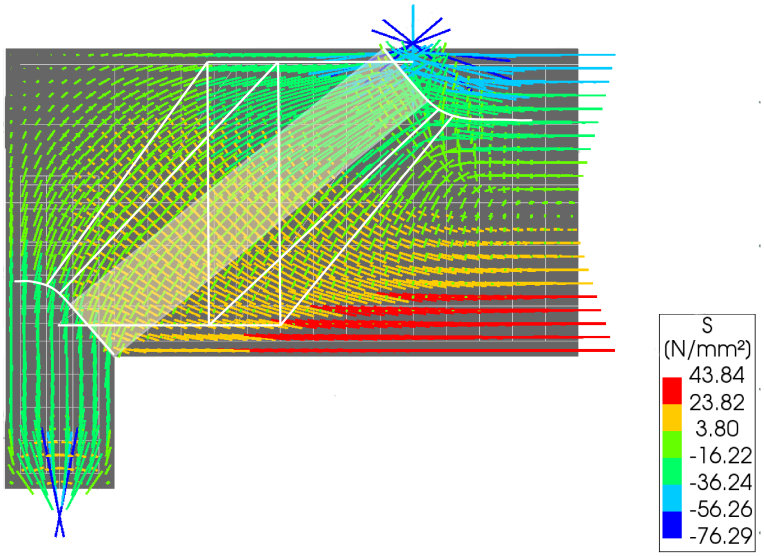

Figure 7: Strut and tie model type 2

In the figure above, a clear strut starting from the point where the force is added till the stub of the beam, is visible. It is also seen that the greatest tensile stresses are at the bottom of the deep beam. With respect to the plot of these stress trajectories, type 2, as described in the paper *"Experimental Studies on High-Strength Concrete Deep Beams"* [2], is chosen as strut-and-tie model. This model is shown on the Figure below.

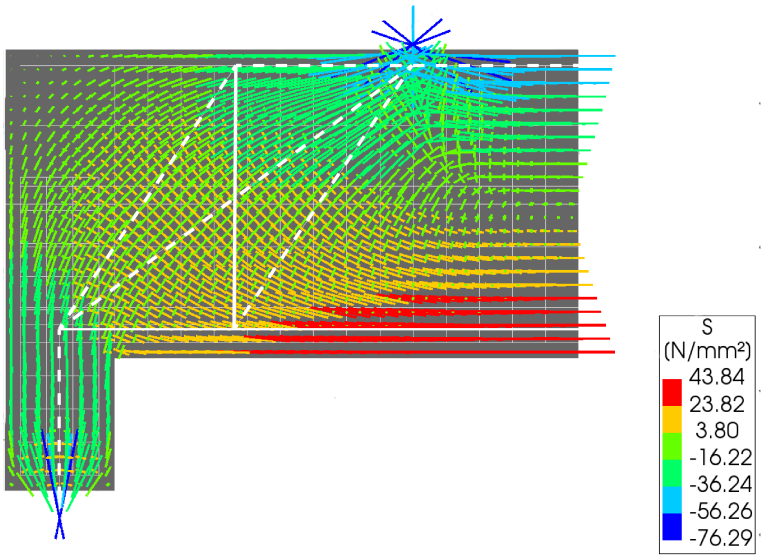

Figure 8: Strut and tie model type 2, with P = - 2 kN

In Figure 9, the composed lines of the strut and tie model are shown. This plot verifies the decision for type 2. One could say that type 3 would also be a possibility for the strut an tie model but as illustrated on the figure, the model with three inclined struts has a better load distribution than compared to type 2. Further it is seen that all the struts are in compression (green) and all the ties are in tension (red).

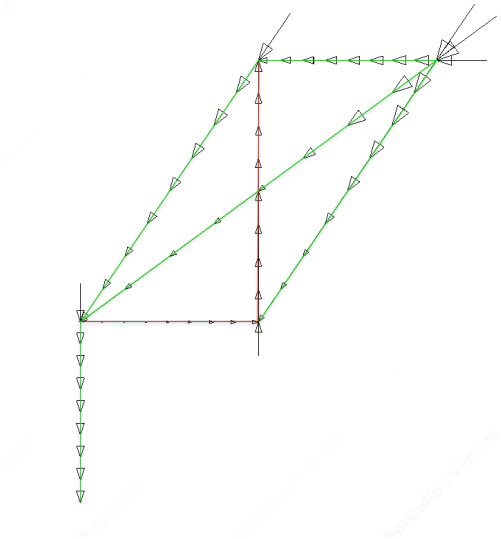

Figure 9: Composed lines of strut and tie model. Green: compression, red: tension

Another way to determine the type of strut and tie model is by looking at the dimensions as done in the paper *Experimental studies on High-strength concrete deep beams* [2]. There the strut and tie model is found by determining the ratio a/z, where a is the shear span and z the internal lever arm. The value of z is assumed to be the distance between the upper compression reinforcement and the centroid of the lower three tension rebars. With this information, the ratio a/z equals 1,361 which means that, according to the discussed paper, the strut and tie model is also of type II (*CEP-FIP Model Code*):

$$\textit{Type II}:$$
$$1 < a/z < \sqrt{3}$$

This confirms the found results based on the stress trajectories from DIANA.

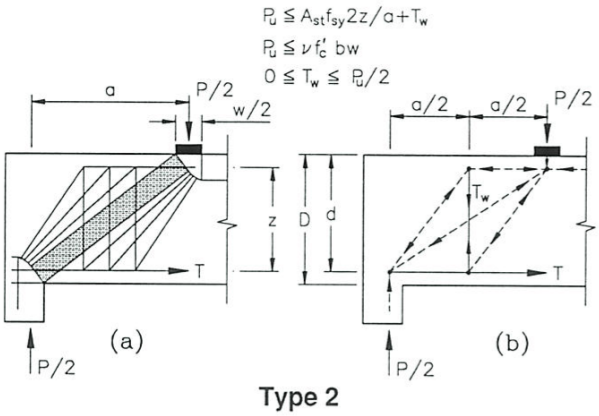

Figure 10: Strut and tie model type 2

3.3 Load bearing capacity

The load bearing capacity of the beam is approximated analytically by using the chosen strut and tie model. The model consists of the following components:

- Struts (concrete)
- Ties (reinforcement)
- Nodes (concrete)

The maximum load capacity of all these elements is verified in order to obtain the overall capacity of the truss model. The stress in struts and nodes is rarely critical so failure due to tension in the middle of the lower tie is expected.

As mentioned before, the internal lever arm is assumed to be 588 mm, which is the distance between the upper reinforcement bar and the central bottom reinforcement bar. Although it would be more complete to determine this value with respect to the neutral axis, these calculations fall beyond the scope of this project.

Normal Forces
First, a force distribution is determined by applying a load P on the truss. The Ritter method is used to compute the individual member forces in the statically determined truss. Figure 11 illustrates the used descriptions of the elements.

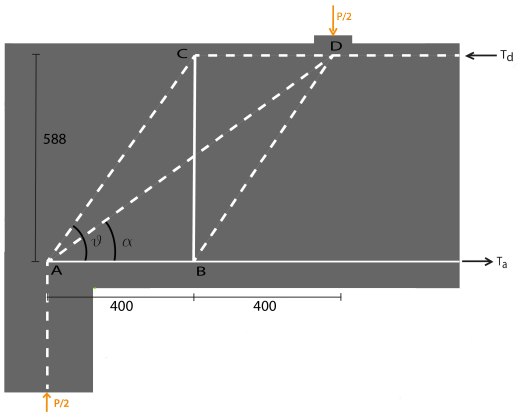

Figure 11: Strut and tie model type 2

Table 8 specifies the contribution of each rod in bearing the force. There it is seen that the bars T_a, AB and CB are in tension and the bars T_d, ad, AC, AD, BD and CD are in compression. This corresponds with Figure 9.

Table 8: Material and design properties

Bar	N
T_a	$0.68027 \cdot P$
T_d	$-0.68027 \cdot P$
AB	$0.58418 \cdot P$
AC	$-0.17085 \cdot P$
AD	$-0.60574 \cdot P$
BD	$-0.17085 \cdot P$
CB	$0.14126 \cdot P$
CD	$-0.09610 \cdot P$

Properties
Subsequently, the material and design properties are defined according to *NBN EN 1992-1-1*. The known parameters are collected in the following table.

Table 9: Material and design properties

Parameter	Value	Unit
a	800	mm
z	588	mm
b	125	mm
θ	55.77	$^\circ$
α	36.32	$^\circ$
f_{cm}	88	N/mm^2
Δf	8	N/mm^2
$f_{y[Y20]}$	440	N/mm^2
$f_{y[W6]}$	590	N/mm^2
γ_s	1.15	-
γ_c	1.5	-
k_1	1	-
k_2	0.85	-
k_2	0.75	-

The cross-sectional widths w of the struts are determined by the size of the nodes and the equations of equilibrium at these nodes. The remaining parameters are computed by the equations below.

$$f_{ck} = f_{cm} - \Delta f = 80\ MPa \tag{1}$$

$$f_{yd[Y20]} = \frac{f_{y[Y20]}}{\gamma_s} = 382.61\ MPa \tag{2}$$

$$f_{yd[W6]} = \frac{f_{y[W6]}}{\gamma_s} = 513.04\ MPa \tag{3}$$

$$f_{cd} = 0.85 \cdot \frac{f_{ck}}{\gamma_c} = 45.33\ MPa \tag{4}$$

$$A_{s[Y20]} = 628.32 \cdot 3 = 1884.96\ \ mm^2 \tag{5}$$

$$A_{s[W6]} = 62.35 \cdot 12 = 374.07\ mm^2 \tag{6}$$

$$v' = 1 - \frac{f_{ck}}{250} = 0.68 \tag{7}$$

Checking Ties
The maximum force P_u that induces failure can now be determined for each tie. The strength in the tension members is taken as the yield strength of the reinforcement.

$$\sigma_{Ed,tie} = \sigma_{Rd,max,tie} \tag{8}$$

$$N_i = A_{s[i]} \cdot f_{yd[i]} \tag{9}$$

The members AB and A are characterised by the 6 longitudinal reinforcement bars indicated by *6Y20* in Figure 10. Tie CB is depicted by 6 sets of stirrups *W6*.

Table 10: Maximum loads P_u per tie

Tie	Maximum load P_u $[kN]$
AB	1234.563
CB	1358.574
A	1060.167

The most conservative value of P_u is the maximum load found according to the resistance of tie A. This means that tension failure occurs in the lower tie as the structure is subjected to the critical value of $P_u = 1060.167\ kN$. As said before, it is expected to be the critical value of the entire model as well. For the sake of completeness and a good understanding, the failure forces of the struts and nodes are determined anyway.

Checking Struts
The struts are checked in a similar way. The compression in the struts must be reduced to below the compressive strength of the concrete. Once again, the maximum force P_u is found by putting the stress in the rod equal to the strength of the element.

$$\sigma_{Ed,strut} = \sigma_{Rd,max,strut} \tag{10}$$

$$\frac{N_i}{w_i \cdot b} = f_{cd[i]} \tag{11}$$

In the bars where there is transverse tension, the compressive strength of the concrete is multiplied by the efficiency factor ν' and 0.6. This results in the following equation:

$$\sigma_{Rd,max,strut} = 0.6 \cdot \nu' \cdot f_{cd} \tag{12}$$

Table 11: Maximum loads P_u per strut

Strut	**Maximum load P_u [kN]**
AC	1662.030
AD	1611.201
CD	7242.426
BD	1662.030
D	2080.500

As predicted before, the struts do not pose a more strict requirement for P_u than the ties.

Checking Nodes
Nodes are typically classified as one of three categories.

- CCC – Pressure-loaded node without reinforcement bars
- CCT – Pressure-Tension node with tie rods anchored in one direction
- CTT – Pressure-Tension node with tie rods anchored in more than one direction

These categories characterize the maximum resistance stress of the nodes.

$$\sigma_{Rd,max,CCC} = k_1 \cdot v' \cdot f_{cd} \tag{13}$$

$$\sigma_{Rd,max,CCT} = k_2 \cdot v' \cdot f_{cd} \tag{14}$$

$$\sigma_{Rd,max,CTT} = k_3 \cdot v' \cdot f_{cd} \tag{15}$$

Lastly, Equation 11 is used one last time to check the maximum bearing capacity of each node. The results are given in table 12.

Table 12: Maximum loads P_u per node

Node A	CCT
Bar	AD
P_u	2282.534 kN
Node B	CTT
Bar	BD
P_u	2077.537 kN
Node C	CCT
Bar	AC
P_u	2354.543 kN
Node D	CCC
Bar	AD
P_u	2685.334 kN

3.4 Comparison and conclusion

Plastic truss and other equilibrium models can be categorised as semi-rational. The model approximates the actual structure on the basis of rational principles. Nevertheless, it is still an approximation. The model ignores a large part of the entire structure and neglects the internal moments and shear forces present in the beam. Stress paths which show the elastic flow of forces are replaced with idealized stress paths with polygons of forces to provide equilibrium. The paper uses the plastic truss model of *Rogowsky and MacGregor* with the effiency factor of *Warwick and Foster*, whereas this report applies the method described in *Eurocode 2*. Deviations between calculations are attributed to this.

Table 13: Comparison of the results

		Paper	**Report**	**Unit**
Exp. Load	$P_{u,exp}$	1550	-	$[kN]$
Plastic Truss model	$P_{u,p'}$	1057	1060.167	$[kN]$
Ratio	$\frac{P_{u,p'}}{P_{u,exp}}$	0.68	0.684	[-]

In the analytical calculations, some safety factors are taken into account. This combined with the fact that the strut and tie model ignores a part of the entire structure, means that the forces will be more concentrated than they really are. A more conservative value of the bearing load capacity in comparison with the experimental result is thus obtained. This is reflected in the ratio seen in Table 13.

4 Non-linear analysis

4.1 Results of a non-linear analysis until failure

Via the non-linear analysis, a load-deflection curve is found and the behaviour at failure is analysed using the crack-pattern and the reinforcement stresses. The values in this analysis are found while using a hexa/quad mesh of 30 mm.

The load scheme is given in Table 14.

Table 14: The load scheme used in the nonlinear calculations

Case	**Loading scheme**
Initial	50.000(15)
Optimised	50.000(10) 5(2) 1(5)

This means that first 15 load steps of 50.000 kN are executed. This analysis is interrupted at a P_u equal to 550 kN. Because a step of 50 kN is not precise enough, the load scheme is optimised to 50.000(10) 5(2) 1(5), with which a more accurate value of $P_u = 513$ kN is achieved.

A remark that must be made is that the loads from the experiment are divided by 2, since it is divided over the two load plates. This means that when the load in the graphs are 1000 kN, the modeled load in DIANA is only 500 kN. A load step of 50 means thus a total increase of 100 kN. The further mentioned forces are the total placed forces, equal to two times the modeled forces.

4.1.1 Load-deflection curve

The load deflection curve can be determined to analyse the load and deflection of the beam at failure. The obtained curve of the lowest node in the middle of the span is compared to the experimental load deflection curve, found in the paper [2]. In Figure 12 and 13, the theoretical and experimental load deflection curves can be found.

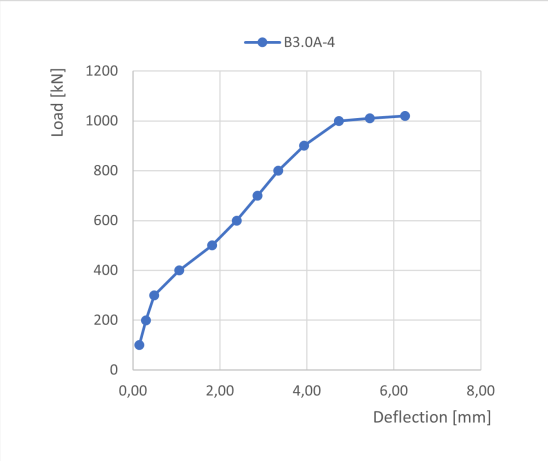

Figure 12: Theoretical load deflection curve

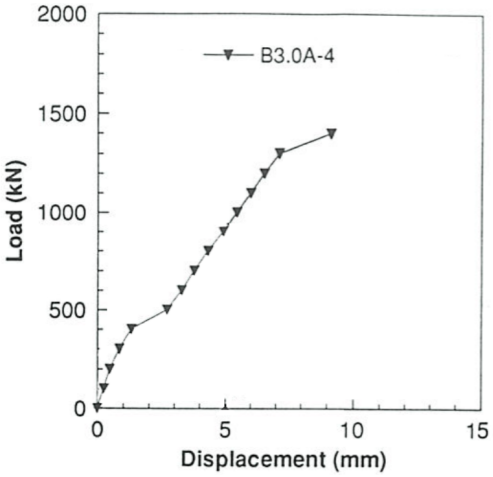

Figure 13: Experimental load deflection curve

As it turns out, their shapes are very similar meaning the behaviour of the beam in the experiment is analog to that of the theoretical model in DIANA. Notice that both the deflections and the loads are smaller since the ultimate load in the theoretical model is around a 1000 kN where in the experimental model a failure load of nearly 1500 kN was achieved. The ultimate displacement of the theoretical model is only around 6 mm where the displacement in the test was approximately 10 mm.

Table 15, found in the previously mentioned paper, compares the different theoretical models to the experimental results. The maximal load that the beam can take is for all the different theoretical models less or more the same and equal to 1000 kN. The "efficiency" of the prediction from the models lies around 60% to 70% meaning that the capabilities of this *B3.0A-4* beam are most often (drastically) underestimated. The strength calculations are thus rather conservative and this might explain why the values of the load-deflection curve are not the same as those of the experiment. The ratio of the P_u obtained with the model is 0.66, which is in line with the theoretical results.

Table 15: Comparison of the experimental results to the theoretical models

Specimen	Exp Load	CIRIA Guide 2		ACI318 - 1989		Plastic Truss Model		
	$P_{u.exp}$ (kN)	$P_{u.c}$ (kN)	$\frac{P_{u.c}}{P_{u.exp}}$	$P_{u.a}$ (kN)	$\frac{P_{u.a}}{P_{u.exp}}$	ν (Eq. 6.11)	$P_{u.p}$ (kN)	$\frac{P_{u.p}}{P_{u.exp}}$
B3.0A-4	1550	944	0.61	1087	0.70	0.480	1057	0.68

Another thing that can be noticed in both load-deflection curves is a kink after the first load steps, as seen in Figure 12 and 13. This means that the beam briefly becomes weaker since the deflection increases more with a given force than before or after this section. Presumably this is because the cracks suddenly increase by a factor 20 in load step 4. This can be seen in the analysis of the cracks further on, where the cracks in phase 3 are a lot bigger than in phase 2.

4.1.2 Reinforcement stresses/crack widths

In this section, different phases of the process are defined, using selected load steps, to explain the failure mechanism of this deep beam. The different phases will be described regarding the reinforcement stresses and the crack widths using the figures below.

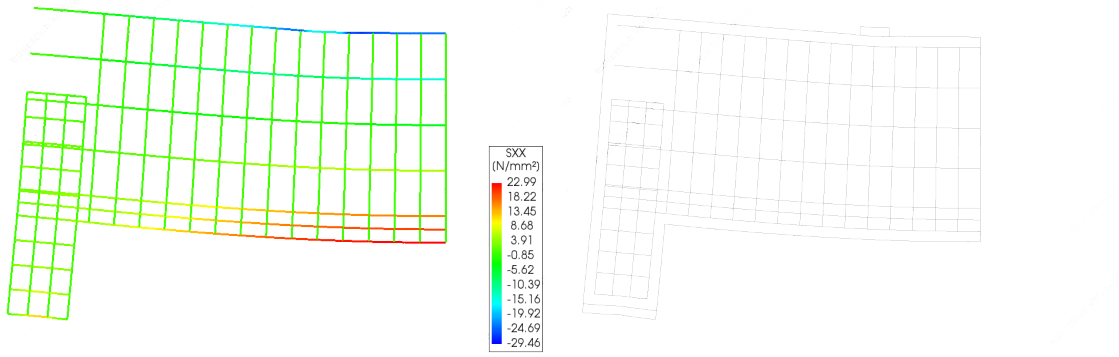

(a) Reinforcement (b) Cracks

Figure 14: Phase 1, no cracks - 200 kN

In phase 1, which corresponds to a load of 200 kN, it can be seen that the tension in the reinforcement is rather minimal. Stresses of around 30 MPa max show up, both in tension and compression. As expected, at the bottom of the beam the steel is tensioned where at the top it is compressed. Notice that in Figure 14, no cracks are present yet.

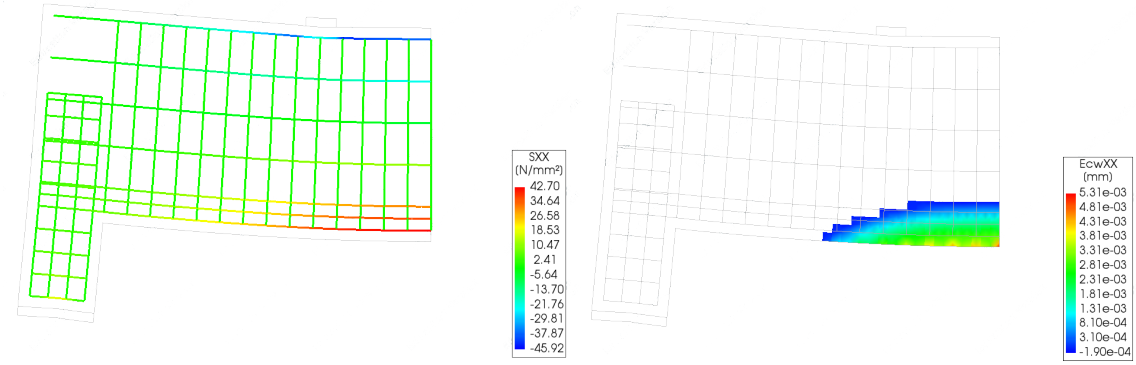

(a) Reinforcement (b) Cracks

Figure 15: Phase 2, cracks starting to form, small local effects in reinforcement bars - 300 kN

The second phase corresponds to a load of 300 kN. The most noticeable aspect about this phase is that the first cracks start to form, but they are not yet visible. The stresses are building up but they are still small.

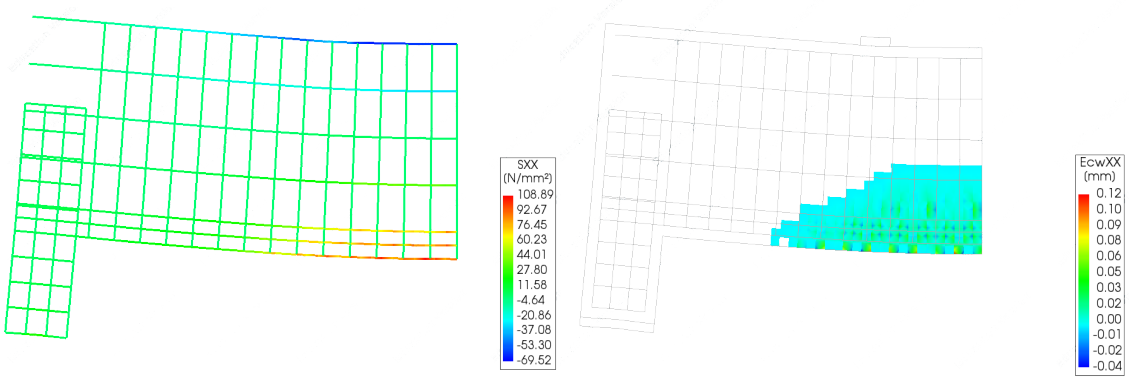

(a) Reinforcement (b) Cracks

Figure 16: Phase 3, cracks are developing - 400 kN

In this third phase, the stresses are increasing and the cracks widths are suddenly becoming a lot larger (also referring to the kink in the load-deflection curve, as discussed in Section 4.1.1). Both the stresses and the cracks are however still within acceptable limits. What's interesting here is that the formation of the cracks leads to some interesting local effects in the stresses of the reinforcement bars. At the bottom reinforcement bars, the steel is alternating between higher and lower tension stresses, caused by the widening cracks.

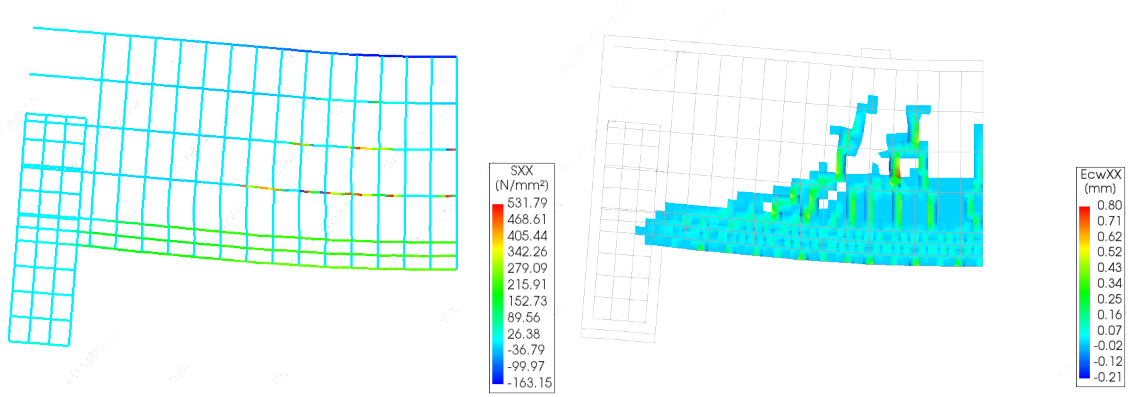

(a) Reinforcement (b) Cracks

Figure 17: Phase 4, bigger cracks, local effects - 700 kN

The load in phase 4 is 700 kN. Local effects due to bigger cracks cause large increases in the stresses and the crack widths. Some small parts of the rebars fail due to overstressing and the crack widths are becoming quite large, while the cracks are reaching to the top of the beam.

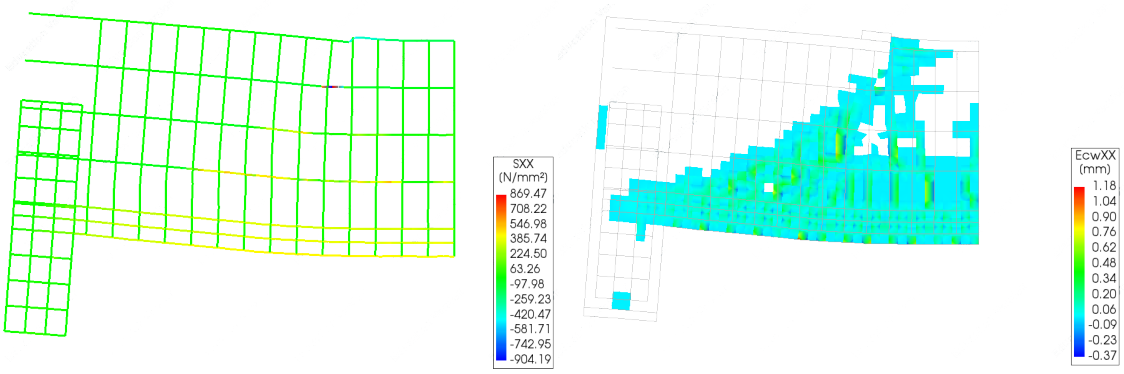

(a) Reinforcement (b) Cracks

Figure 18: Phase 5, moment before failure - 1024 kN

In phase 5, it becomes clear that the largest crack occurs in the connection line between the load plate where the force is applied and the support. This big crack induces huge stress concentrations in the reinforcement. Parts of the middle bars yield, but the beam still has sufficient resistance due to the upper and lower reinforcement and the surrounding concrete at the sides and top as not to collapse.

The cracks in the tension zone are too wide to provide the concrete with any additional strength, which means that all tensile forces are applied to the lower three reinforcing bars. The stresses in the lower rebars are illustrated in Figure 19.

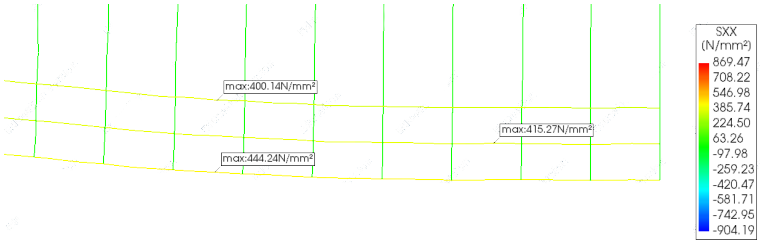

Figure 19: Lower reinforcement bars under a load of 1024 kN

What can be noticed, is that the stresses in the lowest reinforcement bar are already higher than the yield strength, which means it is failing. The two other bars however are still working below yield strength, which makes that the beam doesn't fail.

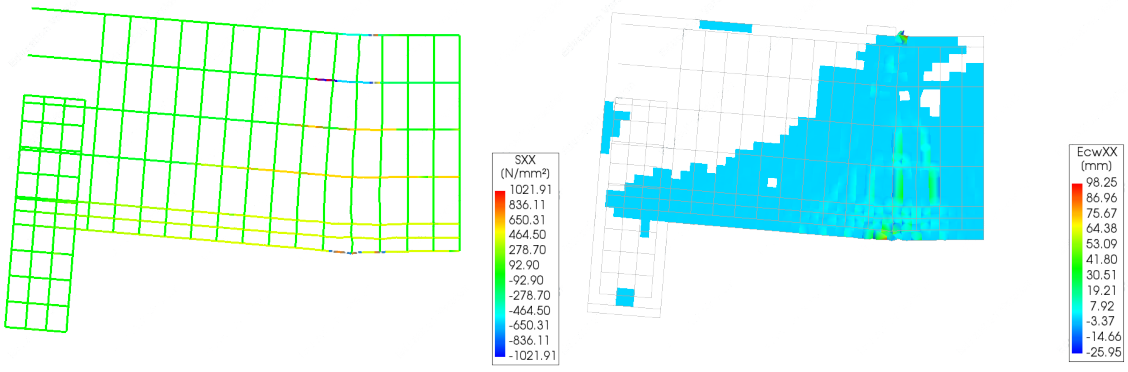

(a) Reinforcement (b) Cracks

Figure 20: Phase 7, failure - 1026 kN

Phase 7 is the situation at failure. Now the reinforcement can no longer provide the beam with the required strength and the beam fails. This is illustrated in Figure 21. All three the lower rebars exceed the yielding stress.

Figure 21: Lower reinforcement bars under a load of 1026 kN, at failure

It is now clear that the failure mode of this beam is in this case tension failure, which is the yielding of bottom reinforcement prior to crushing of the concrete in compression or by web splitting. There is also crushing of the concrete at the top of the beam, but it is not the cause of the failure. This conclusion is in line with the conclusion about the failure mode in the experimental results. When the crack pattern is compared to the one obtained in the experiment (figure 22) the results are again very similar to the crack widths calculated by DIANA.

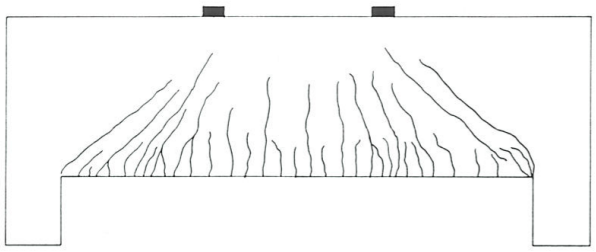

Figure 22: Crack pattern at failure of experimental results

Comparing to the strut and tie model, the same failure mode is observed. Both models fail due to tension failure in the middle of the lower reinforcement rebar. The considered regions of cracks correlate as well.

4.2 Influence of mesh size and type of element

In this last section, the influence of the size and shape of the mesh on the deflection-load curve is investigated. Therefore, six analyses, with two shape types and three different sizes of the elements are executed. Each time, a load-deflection curve is derived in the lowest node of the middle section of the beam. This point is chosen because it undergoes the highest displacements.

4.2.1 Mesh sizes

The determination of the studied mesh shapes is based on the maximum value for the mesh size:

$$\text{element size} = \min\left(\frac{l}{20}, \frac{h}{6}\right) = 52\,\text{mm} \tag{16}$$

Therefore, 10 mm, 30mm and 50mm are chosen to be investigated. The load steps in this analysis are specified for every mesh size, in order to obtain a precise result. In Figure 23, the load-deflection curves of the different mesh sizes and shapes are illustrated.

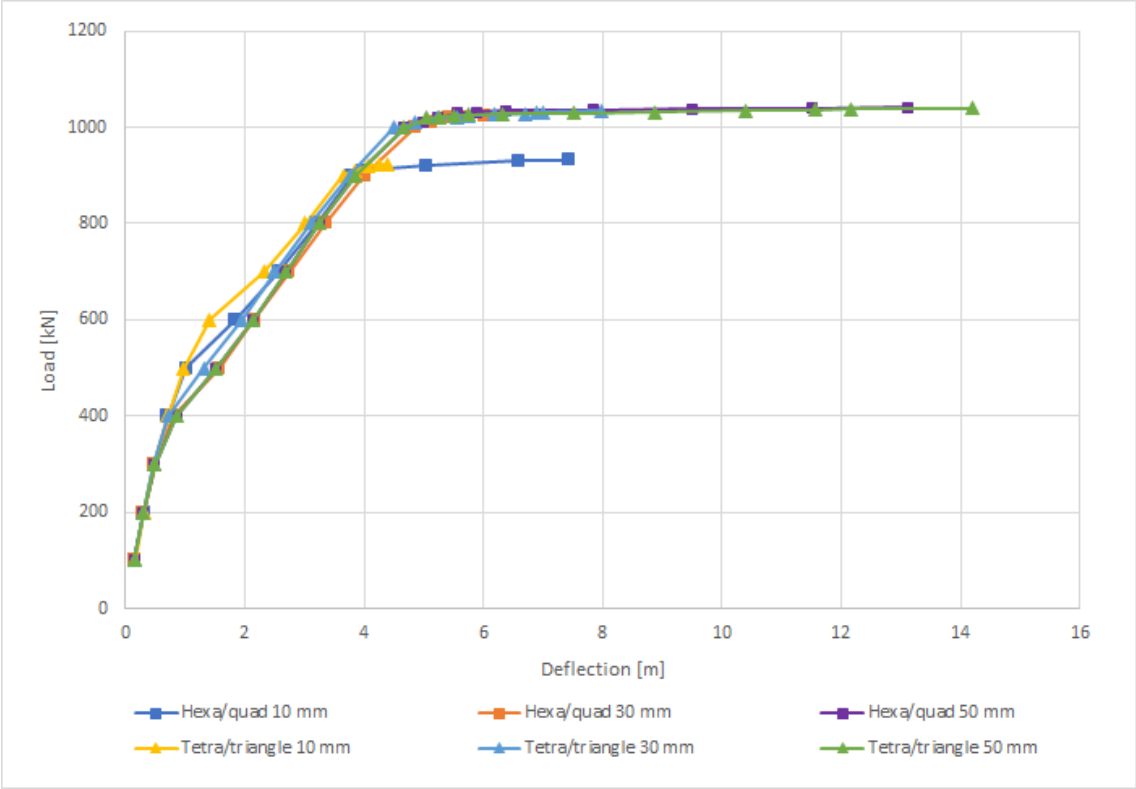

Figure 23: Load-deflection curves of the different mesh sizes and shapes

It can be noticed that the size and shape of the meshes indeed have an influence on the results.

4.2.2 Comparison between sizes/shapes

Taking the extreme cases, it can be noticed that the hexa/quad mesh of 50 *mm* differs quite a lot from the tetra/triangle mesh of 10 *mm* (Figure 24a). This can be expected since both their sizes and shapes differ substantially. It is therefore more useful to compare the sizes and shapes separately. For both shapes it can be seen that the larger the mesh, the larger the deflections (Figure 24b). Comparing the shapes then learns that the hexa/quad shape gives higher deflections than the tetra/triangle shape (Figure 25a and 25b).

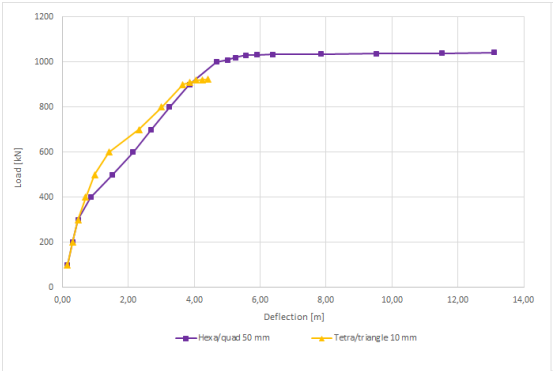

(a) Tetra/triangle 10 *mm* + hexa/quad 50 *mm*

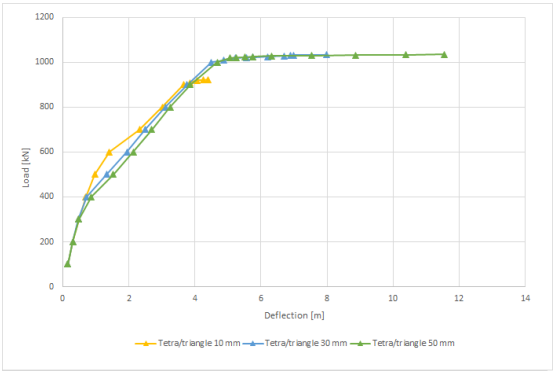

(b) Tetra/triangle 10/30/50 *mm*

Figure 24

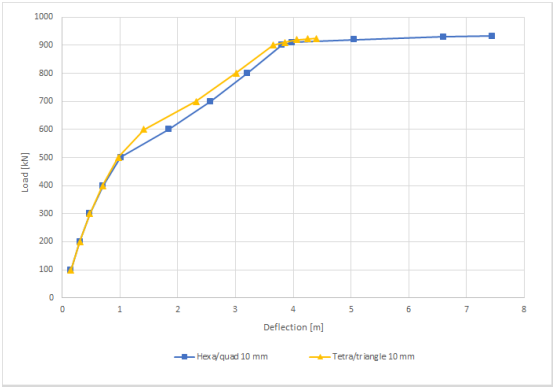

(a) Tetra/triangle 10 mm + hexa/quad 10 mm

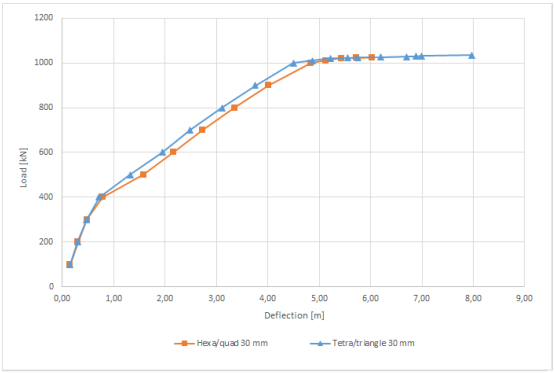

(b) Tetra/triangle 30 mm + hexa/quad 30 mm

Figure 25

Table 16 learns that a smaller mesh gives lower results for P_u. The differences are however not that large.

Table 16: P_u and deflection for different mesh sizes and mesh shapes

	10 mm	**30 mm**	**50 mm**
Hexa/quad	P_u = 1000 kN - 5,63 mm	P_u =1010 kN -7,44 mm	P_u =1008 kN -6,89 mm
Tetra/triangle	P_u =1008 kN - 5,34 mm	P_u = 1018 kN -7,60 mm	P_u = 1020 kN - 12,36 mm

As a small summary, the following remarks can be made:

- The differences between the mesh shapes are (very) small. In Figures 25a, 25b and 26a, the different mesh sizes can be found which show that the smaller the mesh size, the smaller the difference between the shapes becomes.
- The smaller the mesh size, the smaller the deflections and vice versa. This was found in Figures 24b and 26b. It should be noted that the calculation times increase (way) more than linearly with the mesh size. A bigger mesh is therefore preferred over a smaller one because it drastically reduces the calculating time. Also with a decreasing mesh size, the results for P_u become lower.
- The variation of the mesh in the tetra/triangle case is larger than in the hexa/quad case as seen in Figures 26b and 24b. One can conclude that triangular meshes have a higher sensitivity to the mesh size.

4.2.3 Number of elements per mesh shape

To explain the fact that a triangular mesh with the same mesh size as a rectangular mesh gives different results, one can look at the amount of elements that are generated in Table 17. More than double the amount of elements are generated in a triangular mesh versus a rectangular mesh which explains why the triangular mesh compared to the rectangular mesh has a higher sensitivity. Due to the fact that there are so much more elements, this mesh shape should give better results but the calculation time is increased again.

Table 17: Number of elements for the different mesh shapes

Mesh Size [mm]	**Tetra/Triangle**	**Hexa/Quad**
10	22599	9874
30	2462	1063
50	917	399

Triangular meshes assume constant strain within a mesh element while rectangular meshes have a linear strain distribution in one direction. Since in the real beam the strain is not constant, more triangular elements are needed to get the same accuracy as a model with a rectangular mesh. it is therefore concluded that the hexa/quad mesh gives results which are closer towards the experimental results. This can also be seen in the figures because the hexa/quad mesh gives larger deflections which are close to the experimental results either.

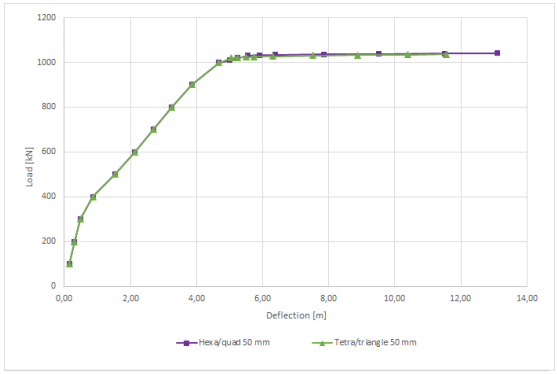

(a) Tetra/triangle 50 mm + hexa/quad 50 mm

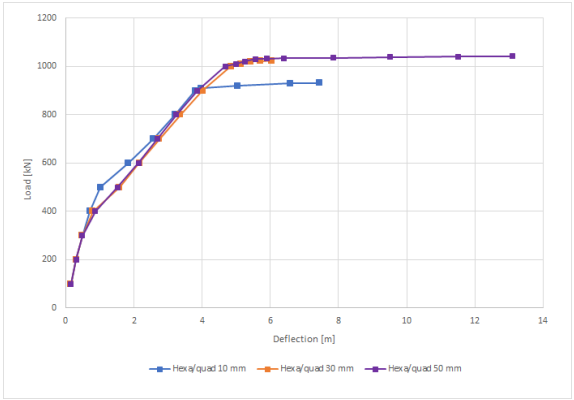

(b) Hexa/quad 10/30/50mm

Figure 26

4.2.4 Conclusion of the non-linear analysis

To conclude this non-linear analysis, it can be stated that a mesh size of 30 mm is a perfect trade-off between calculation speeds and accuracy. Shapewise, the rectangular mesh is preferred since it better represents the real situation and it generates less elements, increasing the calculation speed.

5 Conclusion and summary

In this report, a 2D plane stress model of a concrete deep beam was modeled in DIANA and a FE analysis was performed. First a linear analysis was performed to develop a strut-and-tie model after which a non-linear calculation was performed to check the crack behaviour and tensile stresses.

For the modeling of the beam, the simplification was made to model only half of the geometry because of symmetric and time-efficiency reasons. The different materials with their respective parameters were defined in Section 2.2 before a loading scheme and schedule was proposed in Section 2.3.

In Section 3 then, the linear elastic analysis was performed to obtain the necessary data to develop a strut-and-tie model. First the reaction forces, displacements and stresses were determined after which the stress trajectories were found in order to be able to choose the type of truss-and-tie model. The load bearing capacity was found using this model and the ties, struts and nodes were checked for failure. Ultimately then, in Section 3.4 the achieved results can be found.

After the linear elastic analysis was performed, it was time to move on to the non-linear analysis in Section 4. Again, a loading scheme was chosen from which a load deflection curve was obtained. This was compared to the experimentally found one and despite (slight) deviation in the loads and deflections, both curves showed great resemblance in their shapes. The stresses of the reinforcement and the crack widths were also plotted in different phases to show how the beam behaves under an increasing load and to determine the failure mode. Because of the large number of options regarding the mesh sizes and shapes, their influences were investigated in Section 4.2. It turned out that the differences between the shapes are usually on the smaller side and that the mesh size had a greater influence, especially for the tetra/triangle mesh. It was then concluded that a rectangular mesh of 30 mm seemed to be the golden mean regarding accuracy and calculation time.

6 References

[1] Prof. James K. (2017, 10 maart). Strut-and-Tie Model of a Deep Beam. Civilax. *https://bit.ly/3lnW89T*

[2] Foster, S. J., Gilbert, R. I. (1998). Experimental Studies on High-Strength Concrete Deep Beams. ACI Sturctural journal, 382–390.

[3] Foster, S. J., Gilbert, R. I. (1996). Tests on high strength concrete deep beams. Studies from the school of civil engineering, 1–58.

[4] Rijkswaterstraat ministry of infrastructure and the environment. (2017, juni). Guidelines for nonlinear finite element analysis of concrete structures (2.1).

[5] mpa The Concrete Centre. (2016). Practical Design to Eurocode 2 [Presentation slides]. `https://bit.ly/2VkiEG2`.

[6] Kong, F. K. (2003). Reinforced Concrete Deep Beams. Reinforced Concrete Deep Beams, 1–299. `https://bit.ly/3lrZl8j`

[7] DIANA FEA. (2020). Linear Elastic Analysis of a Deep Beam withWeb Opening (Tutorial). `https://dianafea.com/system/files/deepbeam_104.pdf`

[8] NBN EN 1991. Eurocode 2: Design of concrete structure. - Consulted on 17 December 2020 from, `https://edu.mynbn.be/`

[9] Luc Taerwe. (n.d.). Gewapend beton analyse, modellering en ontwerp. Gent, België: Vakgroepbouwkundige constructies

[10] Prof. Diego Allaix. (n.d.). FEM for linear elastic static problems [Presentation slides]

[11] Dr. Wouter Botte (n.d.). Non-Linear FEM [Presentation slides]